Mitigating Cut Losses in Interdigitated Back Contact Solar Cells

Chen, Ning; Buchholz, Florian; Tune, Daniel D.; Isabella, Olindo; Mihailetchi, Valentin D.

Important note
To cite this publication, please use the final published version (if applicable).
Please check the document version above.

Mitigating Cut Losses in Interdigitated Back Contact Solar Cells

Ning Chen [iD], Florian Buchholz [iD], Daniel D. Tune, Olindo Isabella [iD], and Valentin D. Mihailetchi [iD]

Abstract—The edge recombination losses of crystalline silicon solar cells become significant when they are cut into smaller pieces to be assembled into modules. With the interdigitated pattern of doped p and n regions on the rear side, the interdigitated back contact (IBC) solar cells can be cut through different doped regions. In this study, the cutting losses in IBC solar cells are investigated and various cutting scenarios are studied. Through simulations and experimental measurements, it is found that the cut losses can be reduced by cutting through the back surface field rather than through the emitter. The losses under low light intensity are reduced to an even greater extent. When a 23% cell is cut into 1/3 pieces, the efficiency can be increased by $1.2\%_{rel}$ (cut related losses were improved from $2.0\%_{rel}$ to $0.8\%_{rel}$) under standard 1-sun testing conditions, compared to cutting through the emitter. Under low light intensity of 0.25 sun, the improvement is around $2.4\%_{rel}$. The improvement is mainly due to lower FF losses in the I–V characteristics, and this is further confirmed by Suns–V_{oc} and PL measurements. In the pFF analysis, the additional losses due to laser damage are also observed. This strategy of cutting through the BSF region in IBC solar cells can be quickly adopted in mass production without the need for additional processes or equipment and both module power and energy yield can be increased.

Index Terms—Edge recombination, interdigitated back contact (IBC) cell, laser cutting, low-light performance.

I. INTRODUCTION

THE ongoing industry shift to larger wafer sizes makes the use of cut solar cells in modules a necessity to reduce resistive power losses in strings due to the higher current of the larger wafers. In traditional ribbon-connected modules, half-cut cell modules are already the market's mainstay. Using half-cut cells, the module power is improved by reducing the series resistance losses [1], [2] and the shading behavior is also improved [3]. As the wafer size increases from 156 (M0) to 166 (M6), 182 (M10), and even to 210 (M12), triple-cut cell modules show benefits in terms of both power and efficiency [4]. In the case of modules that use new interconnection technologies, such as shingles, which use small cell stripes that overlap one another, full cells are generally cut into five, six, or more pieces [5]. However, the cutting process introduces additional recombination channels, resulting in a loss of efficiency. In industry, laser cut and cleave (L&C) methods are typically used to cut cells. In this process, a laser is used to cut grooves in solar cells, which are then mechanically cleaved [6]. During the high-power laser process, the wafer surface passivation and silicon bulk in the groove are damaged, and the cleaving process furthermore leaves the wafer edge unpassivated. Losses are dependent upon the ratio of the length of cut edges to the cell area as well as the method of cutting. To maximize the benefits of cut cell technology, it is important to understand the mechanism and extent of losses caused by the cutting process and thus to develop methods for reducing these losses.

Previous studies on cut losses focused mainly on the following three areas.

1) Improving laser cutting techniques to reduce laser damage. In a study by Eiternick et al. [7], it was reported that thermal laser separation (TLS) can reduce the laser damage significantly. According to Kaule et al. [8], the TLS technique also presents an advantage over conventional L&C in terms of mechanical properties. Lelièvre et al. [9] presented a novel ingot cutting methodology in which cells were cleaved according to their crystallographic planes without introducing laser damage.

2) Cutting of various cell structures was also extensively studied, including passivated emitter and rear contact (PERC) [10], n-type passivated emitter rear totally (n-PERT) diffused [11], and silicon heterojunction (SHJ) [12] solar cells. In particular, Baliozian et al. [13] compared the cutting losses in SHJ and PERC cells. In contrast to PERC cells, high-efficiency solar cells, such as SHJ cells, which have a high V_{oc}, result in higher losses.

3) Different strategies for mitigating cut losses have also been extensively investigated. It is possible to repassivate the cut edges by adding an additional layer of passivation [14], [15], [16]. Another promising approach is to introduce a specific pattern at the cell edge by using emitter windows or similar [17], [18], [19] or using laser doping [20].

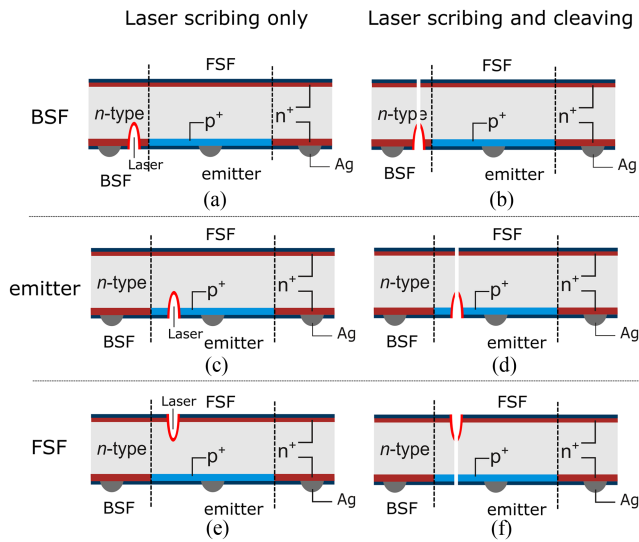Laser scribing only   Laser scribing and cleaving

Fig. 1. Schematic structure (not to scale) of cells with different cutting scenarios. (a) and (b) BSF group: Cuts on BSF and cleaved through the BSF region. (c) and (d) Emitter Group: Cuts on emitter and cleaved through the emitter region. (e) and (f) FSF Group: Cuts on FSF and cleaved through the emitter region.

However, according to our knowledge, there are very few studies regarding cut losses of large-area interdigitated back contact (IBC) solar cells. The reason is may be that the use of cut cells in IBC modules is relatively new. Most of the commercial IBC modules, e.g., as sold by SunPower/Maxeon and LG, are still using the full-cell design, while modules based on half-cut IBC cells have only been available in mass production recently [21]. To reduce the cut losses using the solutions from previous reports would require additional processes and/or equipment that would be challenging to implement in mass production.

In contrast, this article presents a new strategy that can be easily and immediately implemented in mass production and is derived from a detailed study of cut losses in large-area IBC solar cells, and the cell concept based on our commercially available IBC ZEBRA cell [21]. To evaluate the various cutting scenarios and reduce the losses, various simulations and experiments were conducted. The results allow us to propose the new method for effectively reducing recombination losses at the cut edges of IBC solar cells without the need for additional equipment or procedures.

II. MATERIALS AND METHODS

A. IBC Solar Cell Cutting Scenarios and Sample Preparation

In the standard front- and back-contacted cells, laser cutting and subsequent cleaving inevitably occurs through the emitter region, which extends over the entire surface. In contrast, the main feature of IBC solar cells is the interdigitation of the emitter and the back surface field (BSF) regions on the rear of the cells, meaning that they can easily be designed to avoid a cut through the emitter region. Fig. 1 shows the different cutting scenarios for IBC solar cells. The left-hand side column represents the laser scribing process, and the right-hand side column represents laser scribing and additional cleaving processes. Groups are named

as BSF, emitter, and front surface field (FSF). BSF group, as shown in Fig. 1(a) and (b), cuts on BSF and cleaved through the BSF region; emitter group, as shown in Fig. 1(c) and (d), cuts on emitter and cleaved through the emitter region; FSF group, as shown in Fig. 1(e) and (f), cuts on FSF and cleaved through the emitter region.

The following two objectives can be achieved by comparing the different cutting scenarios.

1) By comparing the emitter and BSF groups, the losses due to cutting through the BSF or emitter region can be determined.
2) By comparing the emitter and FSF groups, the role of laser damage in cutting through emitter can be clarified.

In this study, cells were prepared that can be cut from the BSF, emitter, and FSF. In addition, to evaluate the cut-edge effect on different cell sizes, IBC cells have been designed that can be cut into 1/2, 1/3, and 1/4 sizes. All solar cells have been manufactured in our laboratory following the established ZEBRA baseline procedures [22]. The cells were fabricated on 175-μm thick, n-type M2 (length: 156.75 and diameter: 210 mm) wafers with a base resistivity of 4 $\pm$1 Ω·cm. The FSF/BSF and rear emitter regions are formed in industrial tube diffusion furnaces using $POCl_3$ and BBr_3, respectively, as the diffusion sources. A plasma-enhanced chemical vapor deposition mask layer of SiN_x and a 532-nm nanosecond laser were used to form the interdigitated doped regions on the rear side. The passivation and antireflection coating layers were formed by a stacked layer structure comprising thermal SiO_2 grown *in situ* during the diffusion process and capped with SiN_x [23]. Finally, metallization was accomplished using screen-printed 3-D metallization patterns comprising busbars, fingers, and isolation layers. The interdigitated pattern on the rear side was designed such that a doped region of either BSF or emitter was left unmetallized at the designated locations for the final laser scribing process to yield the 1/2, 1/3, or 1/4 size cut IBC cells.

Following the cell processing, a laser was used to scribe the cells to a depth of 50 μm, which is approximately 30% of the cell thickness, followed by manually cleaving the cells into 1/2, 1/3, and 1/4 pieces. For this cutting process, a laser with a plus width of 300 femtoseconds (fs) (Rofin, StarFemto FX) was used. It should be emphasized that although the fs laser was used in this study, other laser sources should produce equivalent results based on our prior findings [24].

In total, nine clusters of cells were fabricated, which included cells of various sizes (1/2, 1/3, and 1/4 cells) and different cutting scenarios (cutting from the BSF, emitter, or FSF, as shown in Fig. 1). In each cluster, there were 11–16 cells.

B. Characterization

The current–voltage (I–V) characteristics were measured under standard test conditions (STCs) for all solar cells to determine the electrical losses induced by the cutting. The measurements were conducted using a commercial AAA-class solar simulator (h.a.l.m. elektronik GmbH). Prior to measurement, the I_{sc} was calibrated using a secondary calibration cell (Fraunhofer

ISE CalLab). The repeatability of the measurement was estimated by repositioning and measuring the same cell five times. In the case of a full cell without laser cutting, the repeatability evaluated by standard deviation divided by average value of different parameters is 0.01% for V_{oc}, 0.08% for J_{sc}, 0.26% for fill factor (FF), 0.02% for pseudo fill factor (pFF), and 0.26% for power conversion efficiency.

To eliminate the effects of light inhomogeneity and probe contact on the measurement of cut cells, which was also reported previously [12], cut cells were measured as "full cells" in this study (i.e., with all cut cells reassembled on the chuck and measured together with their edges not touching). The repeatability of the V_{oc}, J_{sc}, and pFF for cut cell measurements are similar for 1/2, 1/3, and 1/4 cut cells; however, the FF shows different repeatability because the I–V measurement chuck is designed specifically for the measurement of full cells. In terms of repeatability, 1/2 cells are found to be 0.37% for FF and 0.39% for efficiency. 1/3 cells have a repeatability of 0.18% for FF and 0.16% for efficiency. For 1/4 cells, repeatability is 0.60% for FF and 0.56% for efficiency.

During the I–V measurement, the series-resistance-free Suns–V_{oc} curve was measured under a light intensity of 1000 W/m^2. The pFF was extracted from the Suns–V_{oc} curve [25] and was used to further analyze the edge recombination losses without the effect of series resistance [13]. pFF was tested at different stages, i.e., before laser scribing, after laser scribing without cleaving, and after cleaving. pFF was studied specifically for the BSF and emitter groups in order to distinguish the laser effects from different sides. Besides, STC with 1-sun irradiance, a low light intensity test with 0.25-sun irradiance was also conducted. The 0.25-sun irradiance was chosen because of the lowest level achievable in our solar simulator and as a practical limit for which the energy yield of solar modules is still significant. The low-light performance is particularly important, since edge recombination increases with a decrease in light intensity [18], [26]. The low-light performance of solar modules is critical for the energy yield [27], especially for places that experience lower annual irradiance due to geographical and/or seasonal factors.

It has been demonstrated that photoluminescence (PL) characterization is useful in evaluating edge recombination [28], [29]. To validate the electrical measurement, PL measurements were performed on the final cut cells as part of characterization. For the measurement, cells with median FF and efficiency from each group were chosen. Our in-house built PL imaging system was used along with a macrolens to check the PL images of the cut edges, with the same settings as used in the previous study [24]. For the cross-sectional analysis of the cut regions, a laser microscope (Olympus) was used.

C. Simulation

Quokka 3 was used for solar cell simulation, with parameters based on a 23% ZEBRA cell. To speed up the simulation, a unit cell was used rather than a full cell. Different cell sizes were simulated in 3-D, taking into account the dimensions of M2 cells and cutting the cells into 1/2, 1/3, 1/4, and 1/8. Among the cells, half-cut cells were simulated with a single cut edge, and
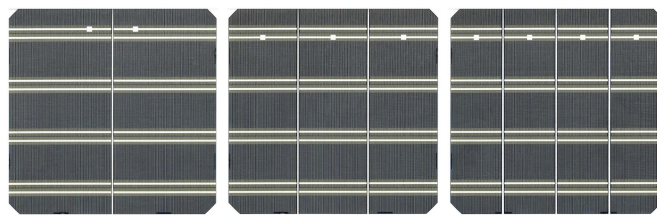

Fig. 2. Photographs of the rear side of solar cells fabricated in this study. From left- to right-hand side: 1/2, 1/3, and 1/4 cells.

1/3 and smaller cut cells were simulated with one cut edge and two cut edges.

In response to cutting through the BSF and emitter regions, two edge structure scenarios were simulated, with the BSF or emitter situated at the edges. There are the following two key parameters of the recombination edges [30].
1) A high-surface recombination velocity value (applicable to all unpassivated edges) of 1.0×10^7 cm/s (e.g., BSF, FSF, and quasineutral bulk regions).
2) If the emitter is cut through, an additional J_{02} emitter recombination current that is assumed to be 19 nA/cm^2 [representing a "worst-case" scenario, assuming a clean but not passivated space-charge region (SCR) recombination surface].

In the simulation, the additional damage caused by the laser is not taken into account. Similar to the experimental part, the I–V characteristics were simulated under both 1- and 0.25-sun irradiance conditions.

III. RESULTS AND DISCUSSION

Fig. 2 shows the rear side of the IBC cells fabricated in this study. As stated in Section II-A, the solar cells were first processed as a whole, and then laser cut and cleaved into 1/2, 1/3, and 1/4 pieces in the BSF, emitter, or FSF cutting scenarios.

To assess edge recombination on various cut cell sizes, the cut edge-to-area aspect ratio (AR) defined by Glunz et al. [18] was used

$$AR = \frac{\text{Laser cut edge length}}{\text{Solar Cell Area}}. \quad (1)$$

In this study, each cut groove creates two laser cut borders, so the laser cut edge length is equal to two times the laser cut number multiplied by the edge length. As examples, the AR of 1/2 cut M2 cells is approximately 0.13 cm^{-1}, 0.26 cm^{-1} for 1/3 cells, 0.39 cm^{-1} for 1/4 cells, and 0.90 cm^{-1} for 1/8 cells, respectively. With this definition of AR, it is possible to extend the findings to other cell sizes, not just the sizes used in this study.

A. Effect of Edge Recombination at 1-Sun Intensity

Solar cells are comparable in terms of their I–V characteristics prior to laser cutting. Table I summarizes the I–V characteristics of each group. Each group contains 11–16 cells.

In contrast, as shown in Figs. 3 and 4, following laser cutting and cleaving, the cells from different groups exhibit different

Group	Cut	V_{oc} (mV)	J_{sc} (mA/cm^2)	FF (%)	η (%)
1/2-cell	FSF	689.6 ±1.8	41.23 ±0.07	80.09 ±0.34	22.77 ±0.16
	emitter	690.2 ±1.1	41.25 ±0.06	80.10 ±0.32	22.81 ±0.13
	BSF	690.2 ±1.2	41.23 ±0.05	80.11 ±0.28	22.80 ±0.10
1/3-cell	FSF	691.1 ±1.6	41.33 ±0.06	79.78 ±0.32	22.79 ±0.13
	emitter	691.9 ±0.8	41.34 ±0.06	79.77 ±0.36	22.82 ±0.11
	BSF	690.9 ±1.2	41.27 ±0.07	79.55 ±0.26	22.68 ±0.14
1/4-cell	FSF	691.2 ±0.9	41.31 ±0.04	80.54 ±0.37	23.00 ±0.12
	emitter	691.0 ±0.7	41.30 ±0.05	80.44 ±0.36	22.96 ±0.09
	BSF	691.0 ±0.9	41.30 ±0.05	80.30 ±0.39	22.92 ±0.14

Fig. 3. Relative losses of $V_{\rm oc}$, $J_{\rm sc}$, FF, and efficiency (η) as a function of AR and cut-through region, under 1-sun irradiance.
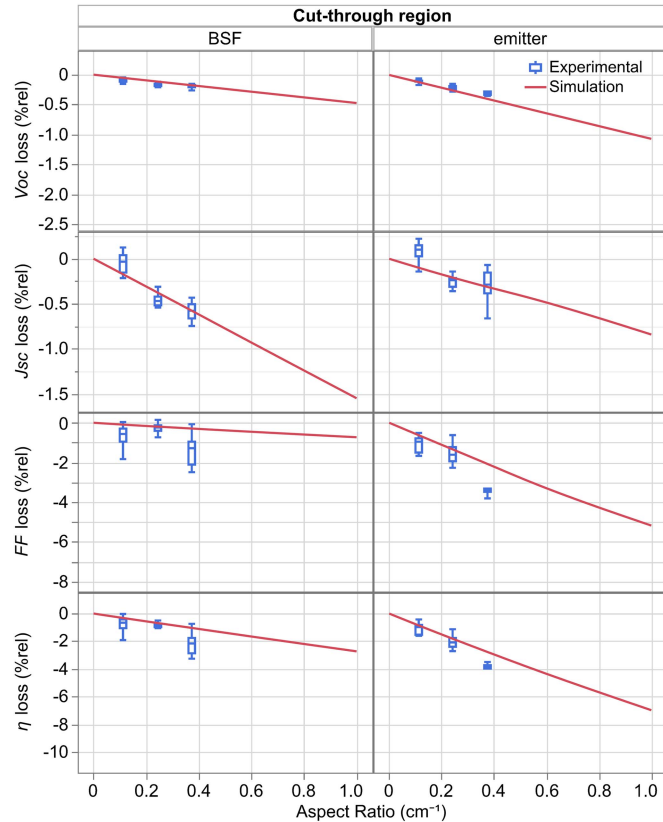

Fig. 4. Relative losses of $V_{\rm oc}$, $J_{\rm sc}$, FF, and efficiency (η) as a function of AR and cut-through region, under 0.25-sun irradiance.

losses, particularly for the group cutting through emitter and the group cutting through BSF.

The experimental mean values of relative losses in main cell parameters are shown in Fig. 3 (symbols) together with the simulated values (lines) as a function of AR and cut region under 1-sun irradiance. The simulated and experimental results agree well for $V_{\rm oc}$ and $J_{\rm sc}$, and the data show that the relative $V_{\rm oc}$ losses are minor. For the 1/4 cells (AR = 0.39 cm^{-1}) cut through the BSF region, an absolute $V_{\rm oc}$ loss of 1.3 mV corresponds to only a 0.20%$_{\rm rel}$ loss, but the losses in the emitter-cut group are slightly higher at around 0.35%$_{\rm rel}$. $J_{\rm sc}$ losses are likewise insignificant. When cut to 1/4 size or smaller, the emitter-cut samples perform marginally better in $J_{\rm sc}$ than the BSF-cut samples, which demonstrates a good current collection on the emitter-cut samples.
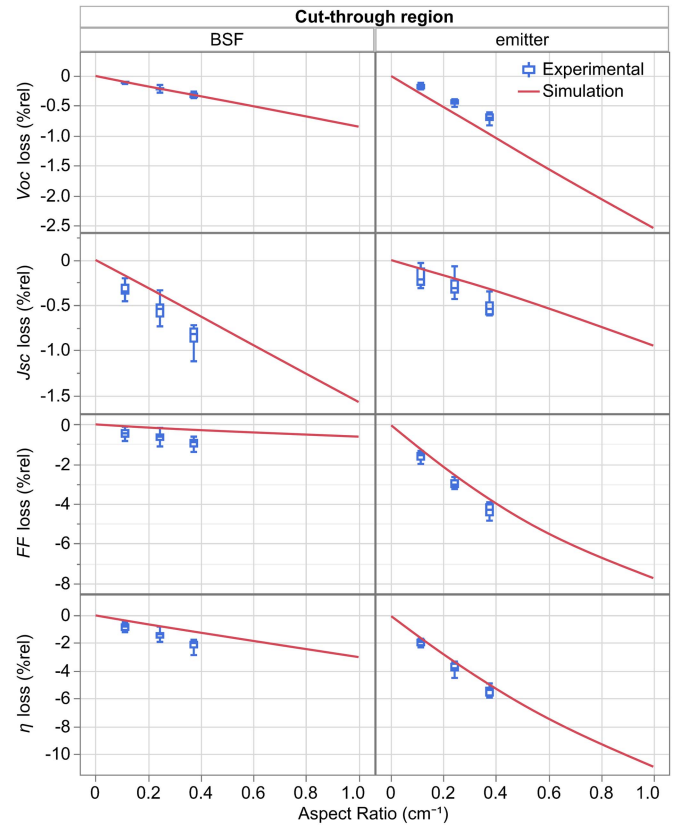
Most of the cut losses can be attributed to losses in the FF. In both simulations and experiments, the losses in the emitter-cut samples are larger than those of the BSF-cut samples as the difference increases with the AR. This shows that edge recombination losses are reduced when cutting through the BSF rather than cutting through the emitter. The higher FF losses observed in the experimental data, in comparison to the simulation, may be due to additional series resistance introduced by the measurement chuck unit, which has been reported previously [8]. A second reason is that the measurement uncertainty of FF is high, particularly when measuring the 1/4 cells, as discussed in Section II-B.

Overall, the BSF-cut group exhibits lower efficiency losses than the emitter-cut group, both in experiment and simulation, and this is mostly due to lower FF losses. In the following discussions, losses are expressed as a relative percentage of the original value (e.g., $J_{\rm sc}$) and differences in losses between different samples are also given. So, cutting through the BSF region rather than the emitter region reduces cut losses by 1.2%$_{\rm rel}$ for 1/3 cells (i.e., 2.0%$_{\rm rel}$ for emitter-cut versus 0.8%$_{\rm rel}$ for BSF-cut).

B. Effect of Edge Recombination at 0.25-Sun Intensity

Fig. 4 shows the relative I–V losses measured at 0.25-sun irradiance, showing similar trends to those obtained under 1-sun irradiance for BSF group. In the emitter group, $V_{\rm oc}$ and FF
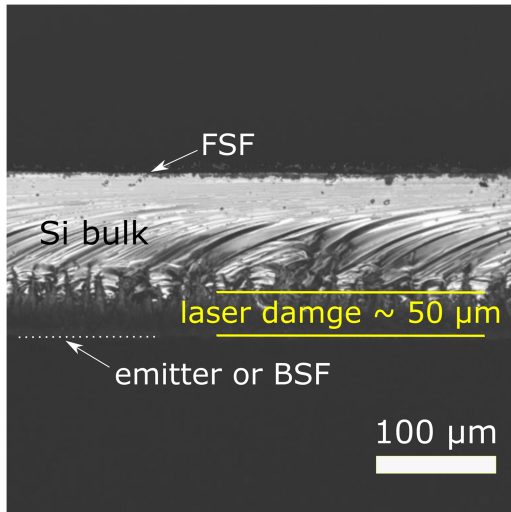
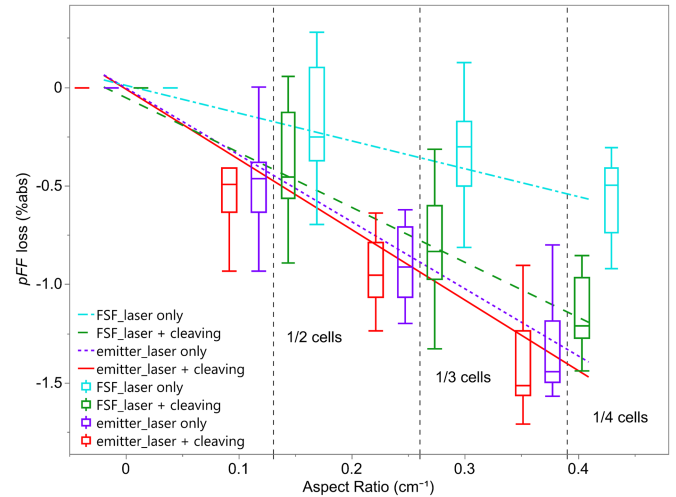Fig. 5.   Cross-section of the laser cutting area.

Fig. 6.   Solar cell pFF losses due to cutting from emitter and FSF sides as a function of AR. The lines are linear fits of the data. The AR corresponding to the cut cell size (1/2, 1/3, or 1/4 cells) is labeled accordingly, and the box plots are with offset from their original positions in order to be distinguished from each other.

losses are greater under 0.25 sun than under 1 sun, while J_{sc} losses remain the same. Therefore, the efficiency gap between the BSF and emitter groups is wider. Thus, the BSF group has gained an advantage of $2.4\%_{rel}$ versus the emitter group for the 1/3 cut cells, both in simulation and in experiments.

C. Effect of Laser Damages

As shown in Fig. 5, the depth of the laser scribe is 50 μm, which is approximately 30% of the wafer thickness. The laser damage thus penetrated through passivation and diffused layers, emitter, BSF, or FSF, which are typically less than 1 μm. Cleaving damage accounts for 70% of the wafer thickness and comprises unpassivated quasineutral bulk edge as well as emitter/SCR or BSF/$n+$ regions.

To further clarify the laser damage losses, the pFF losses for the emitter and FSF groups were analyzed. As shown previously, laser damage can occur on the FSF or the emitter side for the emitter-cut samples. The two groups were measured at different stages. First, before laser scribing without damage; then, after laser scribing without cleaving (with only laser damage), and finally after laser scribing and cleaving (with both laser and cleaving damages). The pFF loss statistics are shown in Fig. 6. A large distribution of data can be seen in the figure, mainly due to measurement uncertainty introduced by the measurement chuck. The chuck used for Suns–V_{oc} was specially designed for full-cell measurement. When cut cells are used, measurement uncertainty increases. However, as we have more than ten samples in each group, the pFF loss can be still analyzed. Trends are clearly visible as shown in Fig. 6.

In the FSF group, around 30%–40% of the pFF loss occurred due to laser damage on the FSF, which is above the laser damage rate of 30%. The main losses in pFF occurred after the FSF-cut wafer had been cleaved. In contrast, for the emitter group in which there is laser damage directly on emitter/SCR, most pFF losses already occurred after laser scribe, with only slight additional pFF losses after cleaving through the bulk and BSF

region. In both groups, the pFF losses due to the exposed SCR regions [31] are clearly observed.

Compared to the pFF losses after cleaving, the FSF group exhibits similar but still lower losses than the emitter group. It was difficult to distinguish the differences between the two groups when cut into 1/2 cells. When the AR is higher, however, the difference between the two groups becomes statistically relevant. A linear fit to the pFF losses in Fig. 6 was applied to show more clearly the laser damage to the SCR regions. These results clearly indicate that laser damage to the emitter region should be avoided during solar cell cutting.

Similarly, researchers have compared the difference between front/emitter and rear/BSF (similarly to FSF-cut in our study) cuts on p-PERC and n-PERT cells [10], [11]. In the report by Xia et al. [11], FF losses were reported (no pFF loss was reported). On half-cut n-PERT cells, FF losses were $1.62\%_{rel}$ when cut on emitter and $0.55\%_{rel}$ when cut on BSF. Münzer et al. [10] reported laser scribe on front-emitter reduced pFF by $7.5\%_{abs}$, when using the L&C technique (M2 PERC cells, cut to 22 mm strips, AR = 0.9). When using TLS, pFF losses were similar between the two. In our study, we only performed L&C cuts. We found that IBC cells have lower pFF losses even when the emitter is cut. There is also a relatively smaller difference between emitter and FSF cuts. In comparison with previous studies, the differences can be explained by both cell structure and laser cutting techniques. It is generally agreed that laser damage to the emitter region should be avoided during the cutting of solar cells.

D. PL Characterization of the Cut Edges

Fig. 7 shows the high-resolution PL images and their corresponding profiles measured with 1-sun equivalent illumination intensity. Cells with median FF and efficiency were selected from each group and measured with PL after laser scribing and
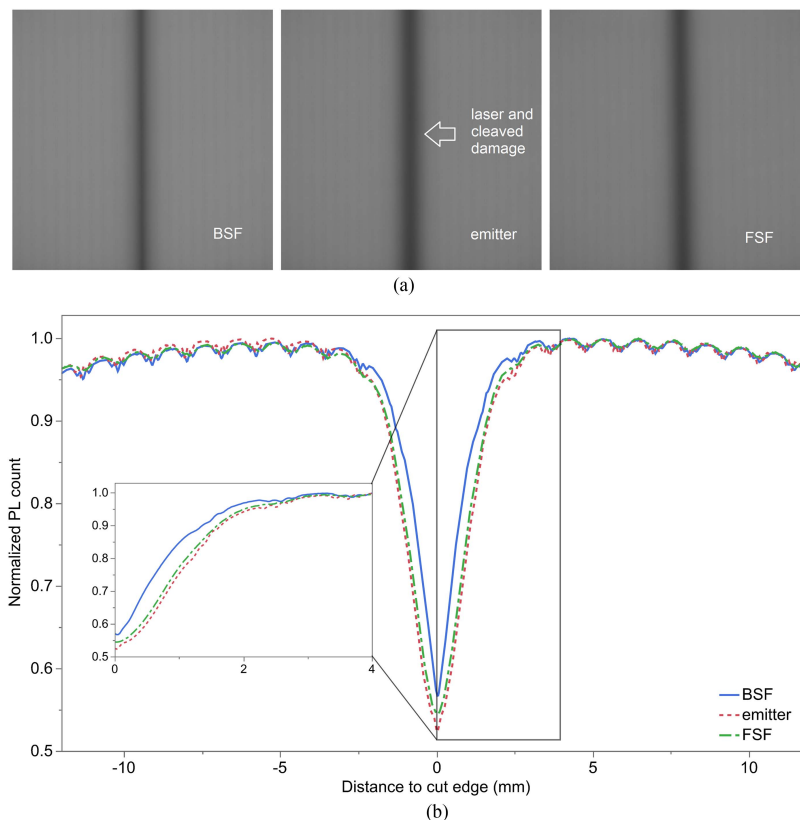
Fig. 7. (a) PL images of the laser cut regions after laser cut and cleaving, with the same scaling. From left to right-hand side: BSF, emitter, and FSF. (b) Cross-section of PL profiles from the cell edge.

cleaving. The line where the L&C were applied is in the center of the images, thus showing the left- and right-hand side cell piece after separation placed next to each other. The PL profiles clearly demonstrate the advantage of cutting from BSF rather than the emitter/FSF, with a steeper profile from the laser cut edge (plot of 0 mm position) to the cell center. Slight differences are also apparent between the FSF-cut and emitter-cut samples. The PL results support the findings of the I–V and pFF results and further demonstrate that the high-resolution PL imaging is a useful tool for qualitatively comparing edge recombination, even at the cell level.

E. Application and the Influence on Module Power and Energy Yield

From the results, it is clear that cutting through the emitter-free BSF regions results in a significant reduction in edge recombination compared to cutting through the emitter. These findings are applicable to all cell concepts based on crystalline silicon (c-Si). However, implementation of the necessary emitter-free cutting regions in a both-sides-contacted cell concept, such as PERC, SHJ, or tunnel oxide passivated contact would require additional process steps for creating the so-called emitter window. The IBC concept thus has an inherent advantage that its doping structures can be designed to avoid emitter cuts without any additional process steps.

The power gains observed on cell level by cutting through the BSF rather than the emitter can be transferred to modules. In this case, both the module power and energy yield are predicted to increase.

In both simulations and experiments, cutting through the BSF results in efficiency losses of $1\%_{\mathrm{rel}}$ or less under 1-sun irradiance for 1/2 and 1/3 cut cells. These losses are small and are comparable to those measured on PERC cells [2], confirming that IBC cells can be used for cut cell modules without additional losses versus similar PERC modules. In the case of a 72-cell M10 module (typically used for power plants) cut into 1/3 cells, the cut losses are reduced by $1.2\%_{\mathrm{rel}}$ or 6.6 W when comparing BSF and emitter cut. For the lower light intensity of 0.25-sun irradiance, the relative efficiency losses improvement by cutting through the BSF instead of the emitter is higher. For the same 72-cell M10 module with BSF cutting, the cut losses are reduced by $2.4\%_{\mathrm{rel}}$ or 3.3 W compared to the module power of around 136 W. As a result of better low-light performance, the energy yield can be improved.

IV. CONCLUSION

An important feature of the IBC solar cell concept is that its doping regions can be designed such that cutting of the cells before module assembly can be done exclusively through either the BSF or the emitter regions. In this article, different cutting scenarios for large-area IBC solar cells were compared using

simulations and experiments. The results clearly showed that cutting through the BSF reduces both FF and efficiency losses compared to cutting through the emitter. Compared to the simulations, higher losses were observed from measurements due to FF effects, as explained in Section III-B; however, the difference in losses between emitter-cut and BSF-cut samples was the same in both simulation and experimental results. Under 1-sun illumination, the measurements of BSF-cut samples showed up to $1.2\%_{\mathrm{rel}}$ reduction in cut losses compared to emitter-cut samples. This reduced the power loss by 6.6 W for a simulated 72-cell M10 module when using 1/3 cut cells. The benefit increases for smaller cell fractions and lower light intensity. In the case of 0.25-sun irradiance, the difference between BSF-cut and emitter-cut is around $2.4\%_{\mathrm{rel}}$. Further investigation reveals that the main pFF losses on the samples cut through the emitter were due to the exposed SCR and that laser damage to the emitter was revealed from linear fitted curves. High-resolution PL measurements also confirmed the I–V and pFF results.

The strategy presented in this work can contribute significantly to reducing the cut losses in IBC cells and modules and markedly enhancing their low-light performance and energy yield. Moreover, this strategy can be easily applied in mass production of IBC cells without the need for additional equipment or processes.

REFERENCES

[1] S. Guo, J. P. Singh, I. M. Peters, A. G. Aberle, and T. M. Walsh, "A quantitative analysis of photovoltaic modules using halved cells," *Int. J. Photoenergy*, vol. 2013, 2013, Art. no. 739374, doi: 10.1155/2013/739374.

[2] J. Müller et al., "Resistive power loss analysis of PV modules made from halved 15.6 × 15.6 cm^2 silicon PERC solar cells with efficiencies up to 20.0%," *IEEE J. Photovolt.*, vol. 5, no. 1, pp. 189–194, Jan. 2015, doi: 10.1109/JPHOTOV.2014.2367868.

[3] K. Brecl, M. Bokalič, and M. Topič, "Annual energy losses due to partial shading in PV modules with cut wafer-based Si solar cells," *Renewable Energy*, vol. 168, pp. 195–203, 2021, doi: 10.1016/j.renene.2020.12.059.

[4] M. Mittag, A. Pfreundt, and J. Shahid, "Impact of solar cell dimensions on module power, efficiency and cell-to-module losses," in *Proc. 30th PV Sol. Energy Conf.*, 2020, pp. 1–6.

[5] D. Rudolph et al., "Cell design optimization for shingled modules," in *Proc. 33rd Eur. Photovolt. Sol. Energy Conf.*, 2017, pp. 880–883, doi: 10.4229/EUPVSEC20172017-2CV.2.44.

[6] S. S. M. Oswald, M. Turek, and J. Schneider, "Evaluation of silicon solar cell separation techniques for advanced module concepts," in *Proc. 28th Eur. Photovolt. Sol. Energy Conf. Exhib.*, 2013, pp. 1807–1812, doi: 10.4229/28thEUPVSEC2013-2CV.4.51.

[7] S. Eiternick et al., "High quality half-cell processing using thermal laser separation," *Energy Procedia*, vol. 77, pp. 340–345, 2015, doi: 10.1016/j.egypro.2015.07.048.

[8] F. Kaule et al., "Mechanical damage of half-cell cutting technologies in solar cells and module laminates," *AIP Conf. Proc.*, vol. 1999, 2018, Art. no. 020013, doi: 10.1063/1.5049252.

[9] J. Lelièvre et al., "Alternative CZ ingot squaring and half-Cell cutting methodology for low-temperature PV cell and module technologies," in *Proc. 37th Eur. Photovolt. Sol. Energy Conf.*, 2020, pp. 487–489, doi: 10.4229/EUPVSEC20202020-2DV.3.7.

[10] A. Münzer et al., "Laser assisted separation processes for bifacial pSPEER shingle solar cells," in *Proc. 37th Eur. Photovolt. Sol. Energy Conf.*, 2020, pp. 394–399, doi: 10.4229/EUPVSEC20202020-2CV.1.51.

[11] L. Xia et al., "Influence of laser cutting conditions on electrical characteristics of half-size bifacial silicon solar cells," *Mater. Sci. Semicond. Process.*, vol. 105, 2020, Art. no. 104747, doi: 10.1016/j.mssp.2019.104747.

[12] F. Gérenton, J. Eymard, S. Harrison, R. Clerc, and D. Muñoz, "Analysis of edge losses on silicon heterojunction half solar cells," *Sol. Energy Mater. Sol. Cells*, vol. 204, 2020, Art. no. 110213, doi: 10.1016/j.solmat.2019.110213.

[13] P. Baliozian et al., "Thermal laser separation of PERC and SHJ solar cells," *IEEE J. Photovolt.*, vol. 11, no. 2, pp. 259–267, Mar. 2021, doi: 10.1109/JPHOTOV.2020.3041251.

[14] P. Baliozian et al., "Postmetallization 'passivated edge technology' for separated silicon solar cells," *IEEE J. Photovolt.*, vol. 10, no. 2, pp. 390–397, Mar. 2020, doi: 10.1109/JPHOTOV.2019.2959946.

[15] A. Münzer et al., "Post-separation processing for silicon heterojunction half solar cells with passivated edges," *IEEE J. Photovolt.*, vol. 11, no. 6, pp. 1343–1349, Nov. 2021, doi: 10.1109/JPHOTOV.2021.3099732.

[16] S. Harrison et al., "Low temperature post-process repassivation for heterojunction cut-cells," in *Proc. 38th Eur. Photovolt. Sol. Energy Conf.*, 2021, pp. 167–171, doi: 10.4229/EUPVSEC20212021-2BO.15.3.

[17] D. König and G. Ebest, "New contact frame design for minimizing losses due to edge recombination and grid-induced shading," *Sol. Energy Mater. Sol. Cells*, vol. 75, no. 3-4, pp. 381–386, 2003, doi: 10.1016/S0927-0248(02)00184-8.

[18] S. W. Glunz et al., "High-efficiency silicon solar cells for low-illumination applications," in *Proc. Conf. Rec. 29th IEEE Photovolt. Specialists Conf.*, 2002, pp. 450–453, doi: 10.1109/pvsc.2002.1190556.

[19] K. Rühle, M. K. Juhl, M. D. Abbott, L. M. Reindl, and M. Kasemann, "Impact of edge recombination in small-area solar cells with emitter windows," *IEEE J. Photovolt.*, vol. 5, no. 4, pp. 1067–1073, Jul. 2015, doi: 10.1109/JPHOTOV.2015.2434597.

[20] C. Chan et al., "Edge isolation of solar cells using laser doping," *Sol. Energy Mater. Sol. Cells*, vol. 132, pp. 535–543, 2015, doi: 10.1016/j.solmat.2014.10.002.

[21] R. Kopecek et al., "ZEBRA technology: Low cost bifacial IBC solar cells in mass production with efficiency exceeding 23.5%," in *Proc. 47th IEEE Photovolt. Specialists Conf.*, 2020, pp. 1008–1012, doi: 10.1109/PVSC45281.2020.9300503.

[22] G. Galbiati, H. Chu, V. D. Mihailetchi, J. Libal, and R. Kopecek, "Latest results in screen-printed IBC-ZEBRA solar cells," in *Proc. 7th World Conf. Photovolt. Energy Convers.*, 2018, pp. 1540–1543, doi: 10.1109/PVSC.2018.8547357.

[23] V. D. Mihailetchi, H. Chu, J. Lossen, and R. Kopecek, "Surface passivation of boron-diffused junctions by a borosilicate glass and in situ grown silicon dioxide interface layer," *IEEE J. Photovolt.*, vol. 8, no. 2, pp. 435–440, Mar. 2018, doi: 10.1109/JPHOTOV.2018.2792422.

[24] N. Chen, D. Tune, F. Buchholz, A. Halm, and V. D. Mihailetchi, "Impact of cut edge recombination in high efficiency solar cells– Measurement and mitigation strategies," in *Proc. 38th Eur. Photovolt. Sol. Energy Conf.*, 2021, pp. 253–256, doi: 10.4229/EUPVSEC20212021-2CV.1.12.

[25] R. A. Sinton and A. Cuevas, "A quasi-steady-state open-circuit voltage method for solar cell characterization," in *Proc. 16th Eur. Photovolt. Sol. Energy Conf.*, 2000, pp. 1152–1155, doi: citeulike-article-id:6901946.

[26] M. Hermle, J. Dicker, W. Warta, S. W. Glunz, and G. Willeke, "Analysis of edge recombination for high-efficiency solar cells at low illumination densities," in *Proc. 3rd World Conf. Photovolt. Energy Convers.*, 2003, vol. B., pp. 1009–1012.

[27] P. Grunow, S. Lust, D. Sauter, V. Hoffmann, and L. Podlowski, "Weak light performance and annual yields of PV modules and systems as result of the basic parameter set of industrial solar cells," in *Proc. 19th Eur. Photovolt. Sol. Energy Conf.*, 2004, pp. 2190–2193.

[28] M. D. Abbott, J. E. Cotter, T. Trupke, and R. A. Bardos, "Investigation of edge recombination effects in silicon solar cell structures using photoluminescence," *Appl. Phys. Lett.*, vol. 88, no. 11, 2006, Art. no. 114105, doi: 10.1063/1.2186510.

[29] D. D. Tune, F. Buchholz, I. Ullmann, and A. Halm, "Measuring and mitigating edge recombination in modules employing cut cells," in *Proc. 37th Eur. Photovolt. Sol. Energy Conf.*, 2020, pp. 322–328, doi: 10.4229/EUPVSEC20202020-2CV.1.13.

[30] A. Fell et al., "Modeling edge recombination in silicon solar cells," *IEEE J. Photovolt.*, vol. 8, no. 2, pp. 428–434, Mar. 2018, doi: 10.1109/JPHOTOV.2017.2787020.

[31] R. Kühn et al., "Investigation of the effect of p/n-junctions bordering on the surface of silicon solar cells," in *Proc. 2nd WCPSEC*, 1998, Art. no. 1390.